Vaid et al., Fig. S1

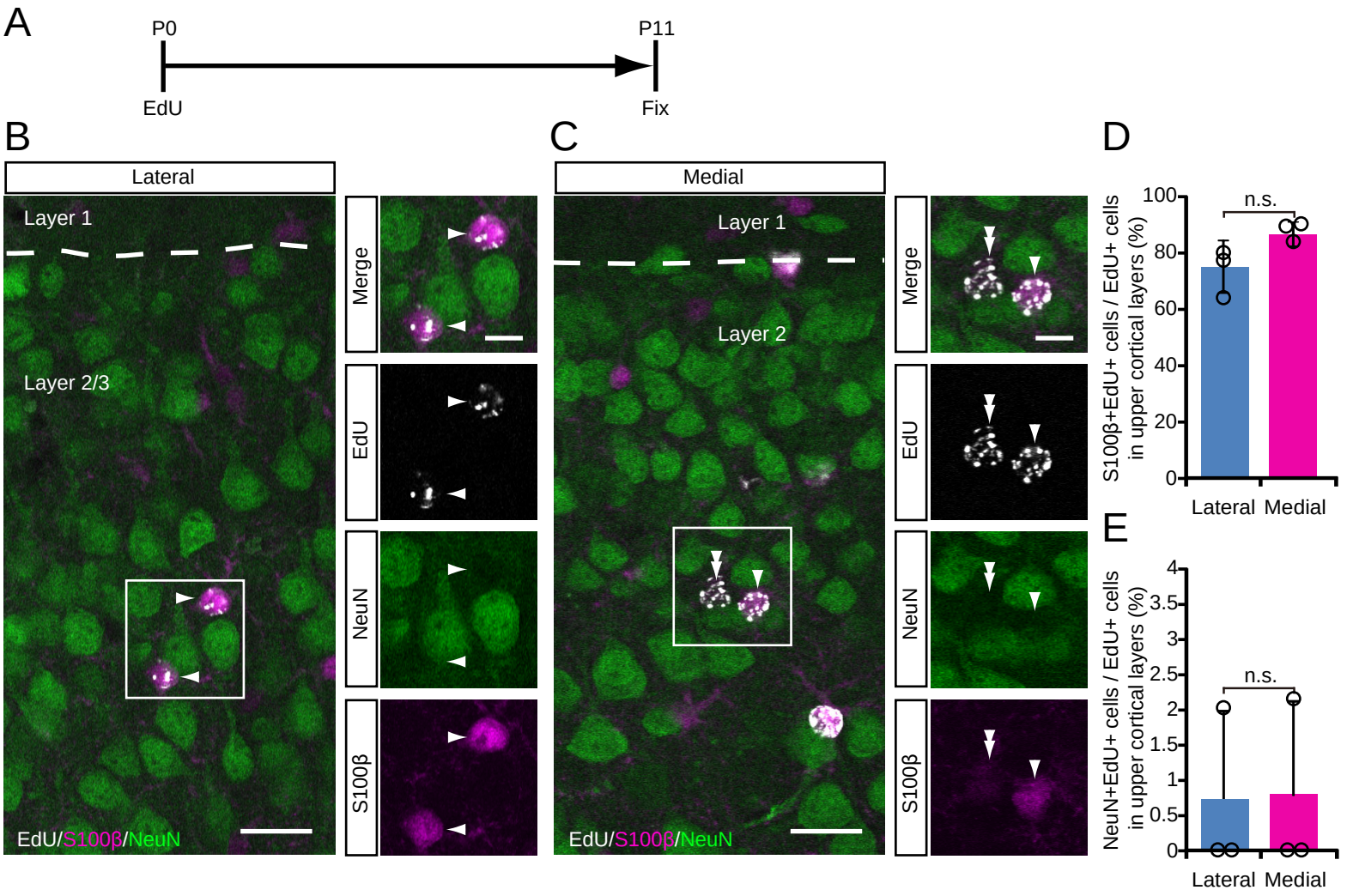

Figure S1. Progenitor cells in mouse P0 latNcx and medNcx give rise mostly to astrocytes.

Mice were labeled by an EdU pulse at P0 and analyzed at P11 (see **A**).

(**B**,**C**) EdU (white), NeuN (green) and S100β (magenta) triple immunofluorescence of cortical layers 2 and 3 (area within 200 µm from boundary between layer 1 and 2 (dashed lines)) of P11 lateral (**B**) and medial (**C**) neocortex. White boxes indicate the areas shown at higher magnification in the respective right panels. Single arrowheads indicate NeuN–S100β+EdU+ cells, and double arrowheads NeuN–S100β–EdU+ cells.

(**D**) Quantification of the percentage of EdU+ cells in the lateral (blue) and medial (magenta) upper cortical layers that are S100β+. Note that most of the EdU+ cells analyzed at P11 following an EdU pulse at P0 expressed the astroglial marker S100ß, indicating that they were the progeny of gliogenic progenitors.

(**E**) Quantification of the percentage of EdU+ cells in the lateral (blue) and medial (magenta) upper cortical layers that are NeuN+. Note that hardly any NeuN+ EdU+ neurons were detected at P11 following an EdU pulse at P0.

(**D**,**E**) Error bars indicate SD; n.s., not statistically significant; Welch's *t*-test in **D** (n = 3 mice, $P = 0.15$, $\varphi = 2.78$, $t = -1.96$), and Mann–Whitney U-test in **e** (n = 3 mice, $P = 0.32$). Open circles in the bar graphs in **D** and **E** represent individual data points.

(**B**,**C**) Images are single 0.4-µm optical sections; scale bars, 20 µm (left panels in **B**,**C**) and 10 µm (right panels in **B**,**C**).

Vaid et al., Fig. S2

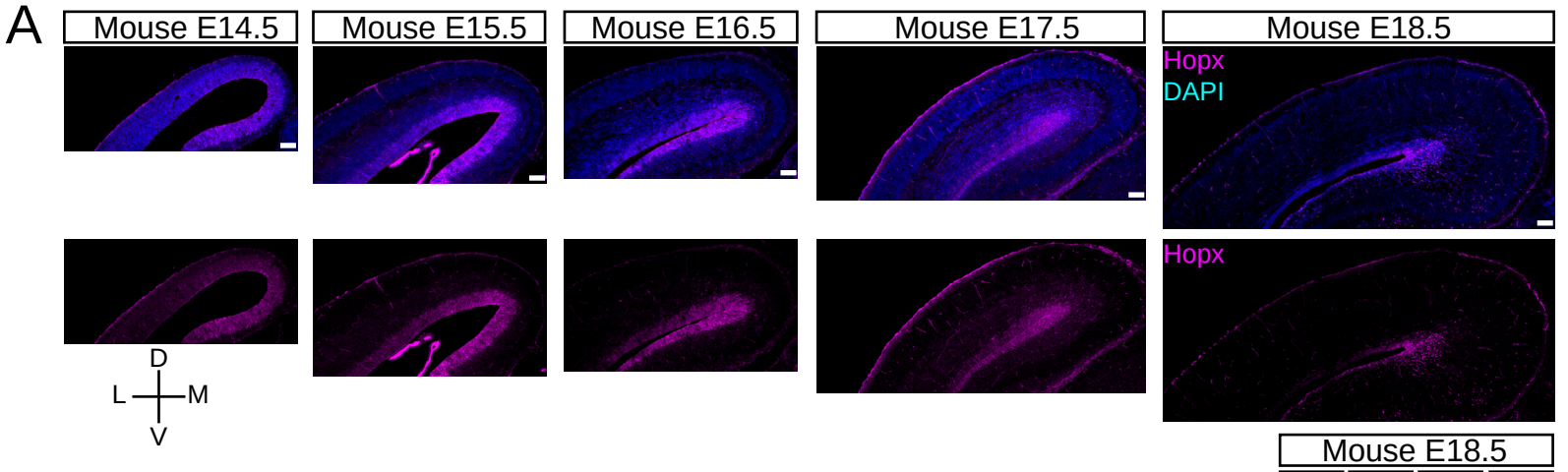

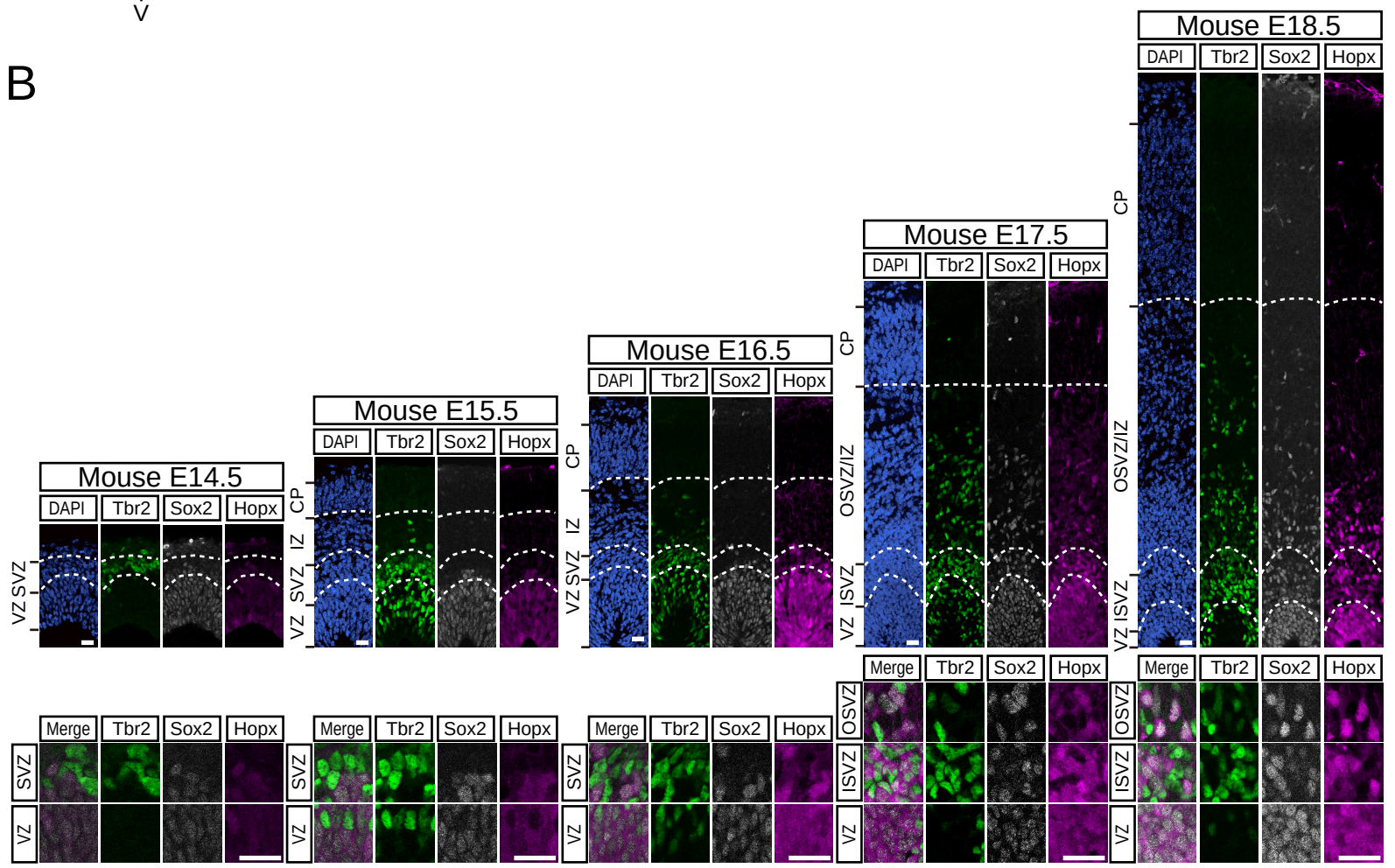

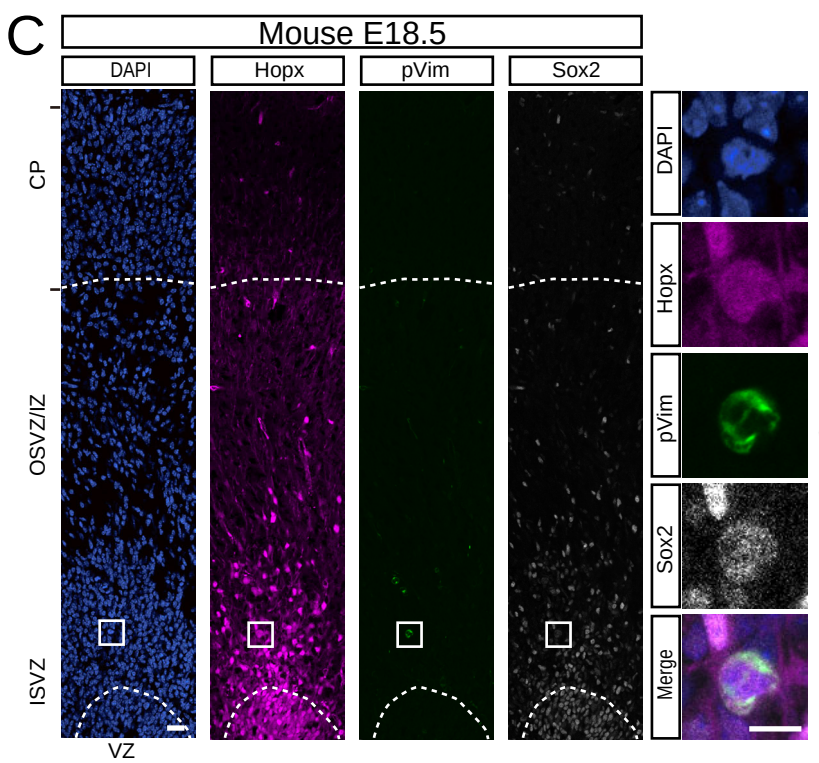

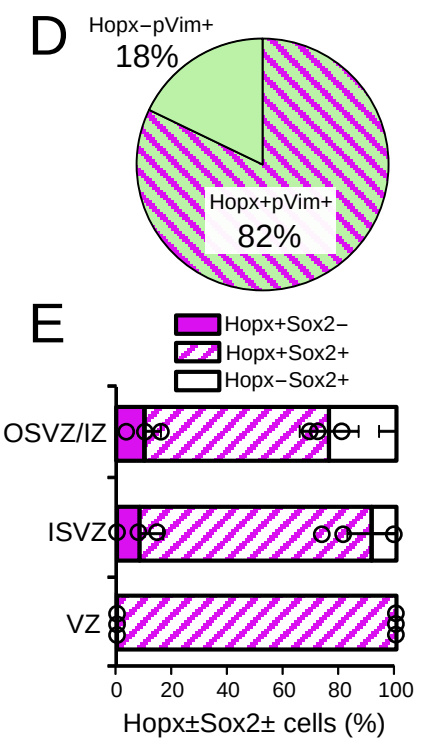

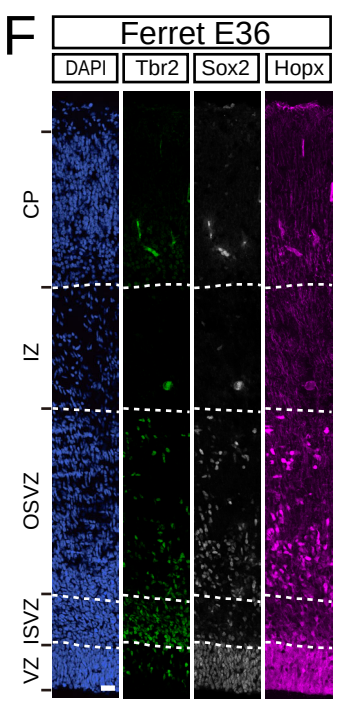

Figure S2. Pattern of Hopx expression in the embryonic mouse and ferret neocortex.

(**A**) Hopx immunofluorescence (magenta), combined with DAPI staining (blue), in the mouse neocortex at E14.5, E15.5, E16.5, E17.5 and E18.5. D, dorsal; M, medial; V, ventral; L, lateral.

(**B**) Hopx (magenta), Sox2 (white) and Tbr2 (green) triple immunofluorescence, combined with DAPI staining (blue), in the mouse medNcx at E14.5, E15.5, E16.5, E17.5 and E18.5. Dashed lines indicate the boundaries between VZ, SVZ, IZ, ISVZ, OSVZ/IZ and CP. Lower panels show higher-magnification images of VZ, SVZ, ISVZ and OSVZ.

(**A,B**) Note that Hopx immunoreactivity in the latNcx was detected at a low level in the VZ at E14.5 but decreased with the progression of neocortical development and eventually disappeared by E18.5. In contrast, in the medNcx, which was immunostained for Sox2 and Tbr2 to distinguish VZ, ISVZ and OSVZ, Hopx immunoreactivity in the VZ increased from E14.5 until E18.5 and became detectable in the ISVZ and OSVZ at E17.5. Note further that these dynamics of Hopx expression in developing mouse medNcx are similar to what has been reported for fetal human neocortex, where during early gestation (GW13.5) Hopx+ cells are present mainly in the VZ, whereas later in gestation (GW14.5) Hopx+ cells are present also in the ISVZ and OSVZ(Pollen et al., 2015).

(**C**) Hopx (magenta), pVim (green) and Sox2 (white) triple immunofluorescence, combined with DAPI staining (blue), in the mouse E18.5 medNcx. White boxes in the

left panels indicate the areas shown at higher magnification in the right panels. Dashed lines indicate the boundaries between VZ, ISVZ-OSVZ/IZ, and CP.

(**D**) Quantification of the percentage of basal pVim+ cells that are Hopx+ (green with diagonal magenta lines) and Hopx– (green only) in the mouse E18.5 medNcx.

(**E**) Quantification of the percentage of cells that express Hopx and/or Sox2 in the indicated zones of the mouse E18.5 medNcx; Hopx+Sox2– (solid magenta), Hopx+Sox2+ (diagonal magenta lines) and Hopx–Sox2+ (solid white). Error bars indicate SD. Open circles in the bar graph represent individual data points (n = 3 embryos); note that the sum of the three cell populations was set to 100% for each of the three embryos.

(**F**) Hopx (magenta), Sox2 (white) and Tbr2 (green) triple immunofluorescence, combined with DAPI staining (blue), in the ferret E36 latNcx. Dashed lines indicate the boundaries between VZ, ISVZ, OSVZ, IZ and CP.

(**A**,**B**,**C**,**F**) Images in **A** are single 4.3-µm optical sections, images in **B**,**C** and **F** are single 0.6-µm optical sections; scale bars, 100 µm (**A**), 20 µm (**B** and left panels in **C**), 10 µm (right panels in **c**), and 50 µm (**F**).

Vaid et al., Fig. S3

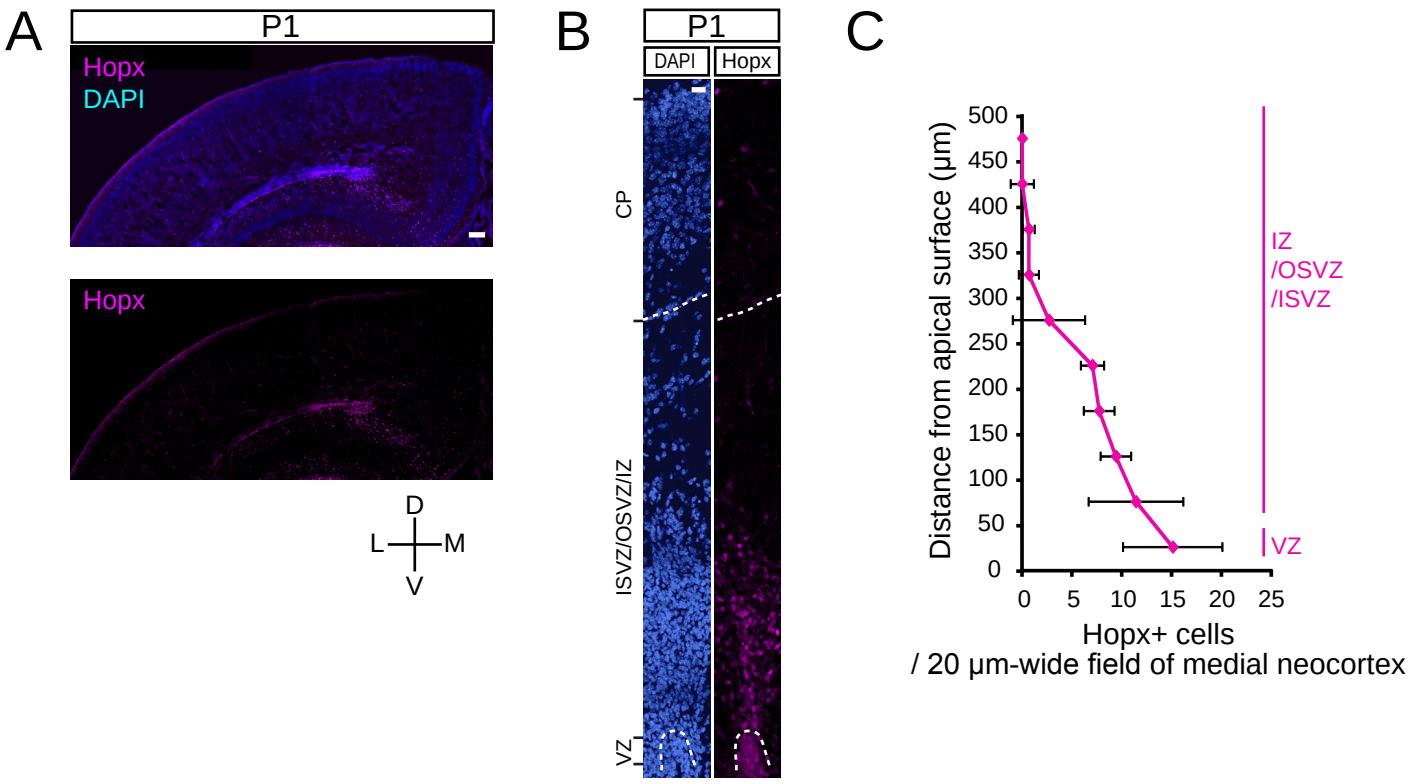

Figure S3. Expression of Hopx in the early postnatal mouse neocortex.

(**A**) Hopx immunofluorescence (magenta), combined with DAPI staining (blue), in the mouse neocortex at P1. D, dorsal; M, medial; V, ventral; L, lateral.

(**B**) Hopx (magenta) immunofluorescence, combined with DAPI staining (blue), in the mouse medNcx at P1. Dashed lines indicate the boundaries between VZ, ISVZ/OSVZ/IZ and CP.

(**C**) Quantification of the distribution of Hopx+ cells along a 500-µm radial axis (divided into 10 bins) of the medNcx (20 µm-wide field) at P1. Error bars indicate SD.

(**A**,**B**) Images in **A** are 17-µm merged stacks (7 partly overlapping single 4.3-µm optical sections), images in **B** are single 0.6-µm optical sections; scale bars, 50 µm (**A**) and 20 µm (**B**).

Vaid et al., Fig. S 4

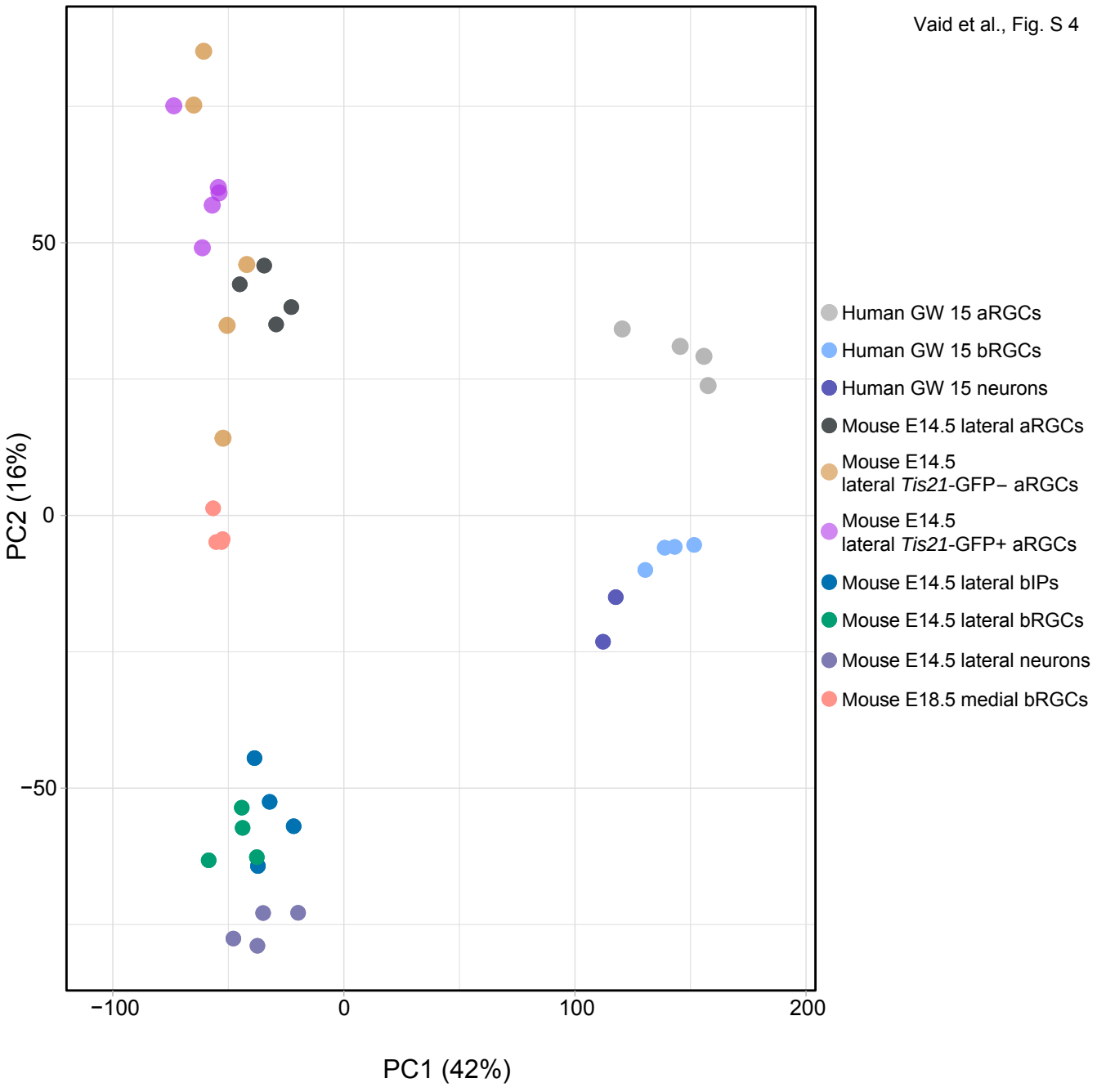

Figure S4. PCA of RNAseq data obtained from various isolated mouse and human cortical progenitor cell populations and neurons.

PCA of RNA-seq data of (i) bRGCs isolated from mouse E18.5 medNcx (this study), (ii) cortical progenitor populations isolated from mouse E14.5 latNcx (Florio et al., 2015) (GSE65000), and (iii) bRGCs isolated from human GW15 neocortex (Florio et al., 2015) (GSE65000), as indicated by the various colored dots (4-5 replicates per cell population). The percentages of variance explained by PC1 and PC2 are indicated. Note that the greatest difference between these cortical cell populations was between mouse and human cell populations, as revealed by PC1, and that the next greatest difference was between human aRGCs vs. human bRGCs and neurons, and between mouse lateral aRGCs, *Tis21*-GFP– negative and –positive aRGCs vs. mouse medial bRGCs vs. mouse lateral bRGCs, bIPs and neurons, as revealed by PC2.

Vaid et al., Fig. S5

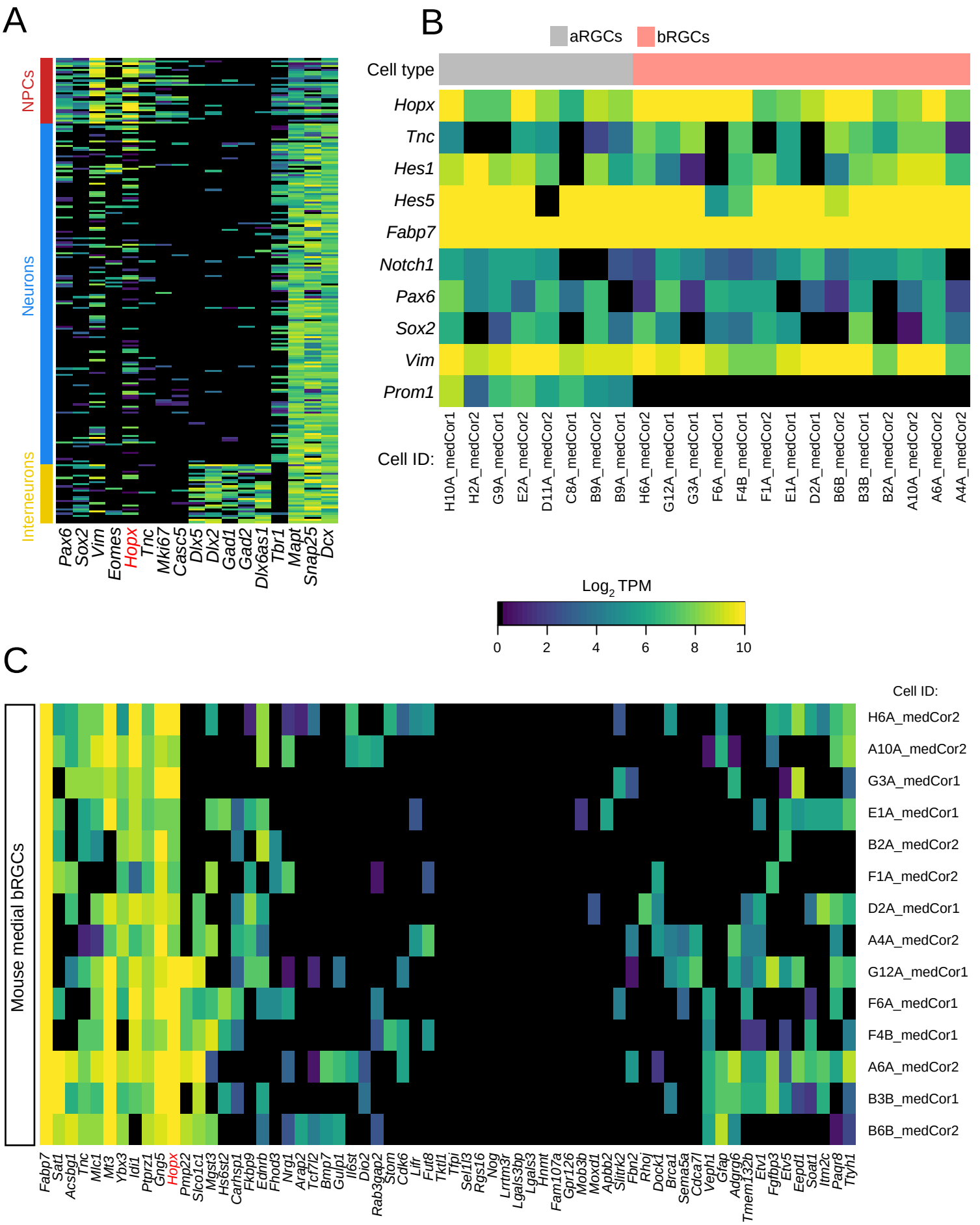

Figure S5. Single-cell RNA-seq of cells isolated from mouse E18.5 medNcx.

Single-cell RNA-seq analysis on 221 disscociated cells obtained from microdissected mouse E18.5 medNcx (two independent analyses using a pool of 8 neocortices each).

(**A**) Heatmap of expression of selected genes expression in individual cells. PCA was used to identify cell populations. Cells are in rows, genes in columns. Color codes for cell populations: NPCs (31 neocortical progenitor cells, red), excitatory cortical neurons (162 cells, blue), interneurons (28 cells, yellow).

(**B**) Heatmap of selected radial glia marker gene expression in the 22 neocortical progenitor cells that express *Hopx* >5 in Log_2 TPM. aRGCs (grey, 8 cells) and bRGCs (red, 14 cells) are separated based on the absence (black) or presence (colors) of *Prom1* expression. Cells are in columns, marker genes in rows.

(**C**) Heatmap showing the expression of the 64 mouse orthologs of the human bRGC-enriched genes (Pollen et al., 2015) in the 14 bRGCs identified in (**B**). Cells are in rows, genes in columns. Note that essentially all of these cells showed detectable expression of most, if not all, of these 64 genes.

(**B**,**C**) The last number of the cell ID indicates from which of the two independent experiments the cell originated.

Vaid et al., Fig. S6

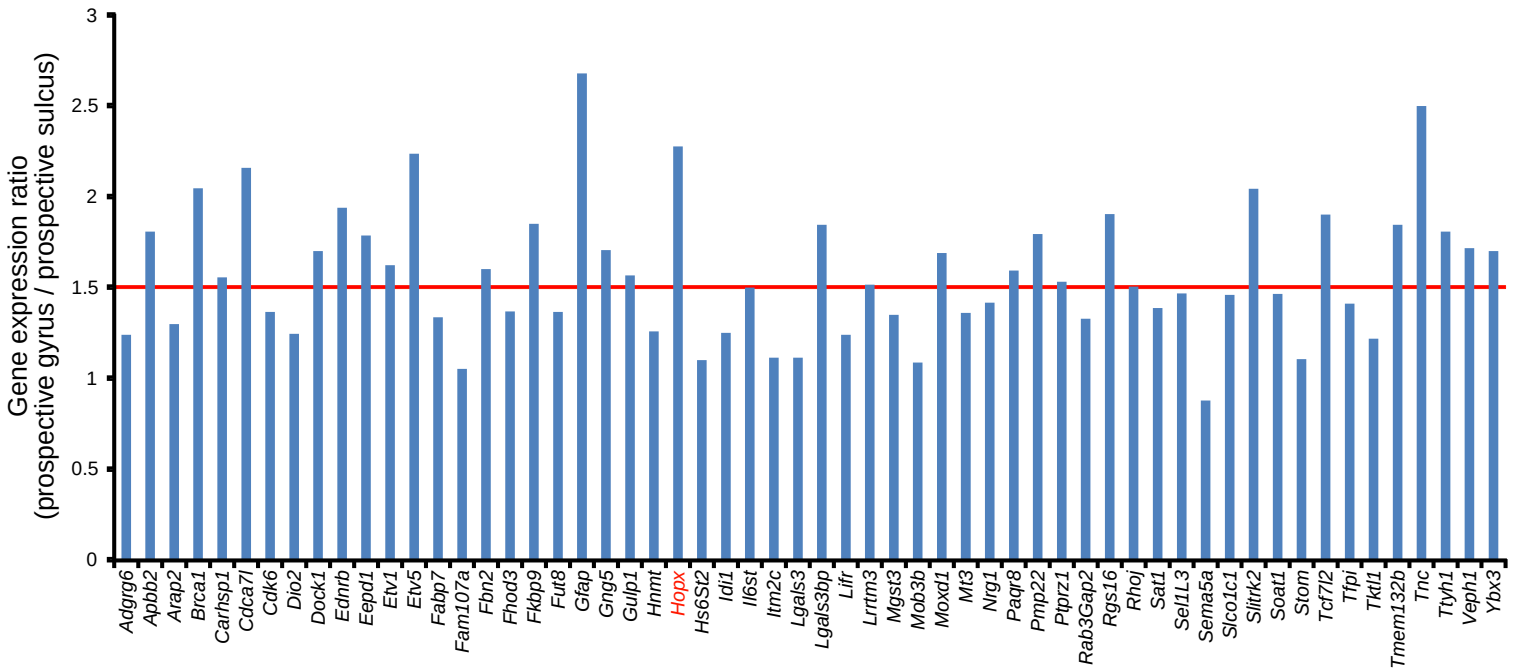

Figure S6. Expression of human bRGC-enriched genes in the OSVZ of developing ferret neocortex.

Gene expression levels of 58 of the 64 human bRGC-enriched genes (Pollen et al., 2015) in the P2 ferret OSVZ are expressed as prospective gyrus / prospective sulcus ratio. Microarray data are from a previous publication (De Juan Romero et al., 2015) (GSE60687). Red line indicates a ratio of gene expression levels of 1.5. Note that 30 genes show an at least 1.5-fold greater expression level in the OSVZ of the prospective gyrus than the OSVZ of the prospective sulcus.

Vaid et al., Fig. S7

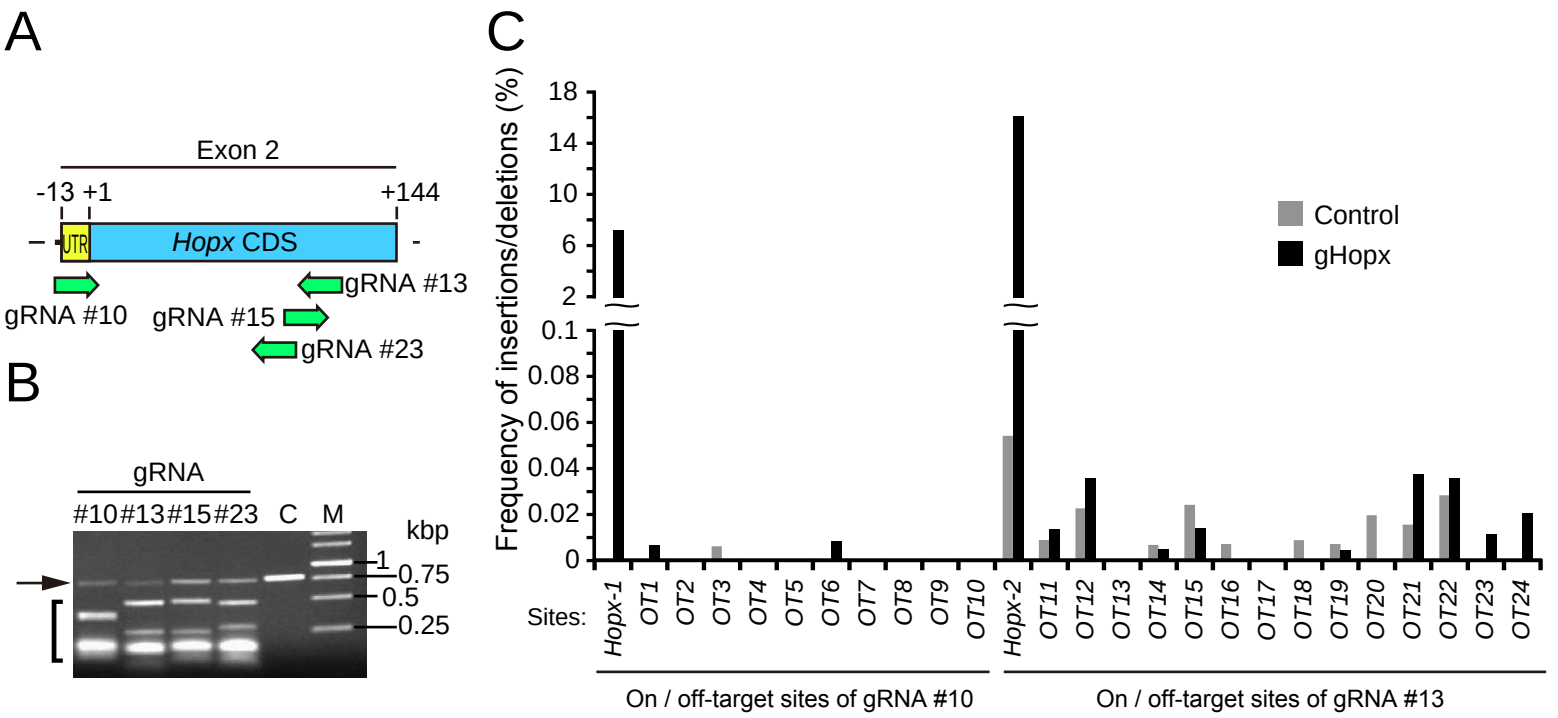

Figure S7. CRISPR/Cas9-mediated disruption of Hopx expression in the embryonic mouse medNcx and its effect on the level of mitotic BPs.

We established CRISPR/Cas9-mediated disruption of Hopx expression in mouse embryonic neocortex, using a mixture of two guide RNAs (gRNA #10 + gRNA #13) (see panels A-E). An analysis of the distribution of the intensity of Hopx immunoreactivity in these cells between control and gHopx electroporation allowed us to identify a threshold level above and below which cells were defined as Hopx+ and Hopx–, respectively (see Methods and panel F).

(**A,B**) Schematic diagram of exon 2 (157 nt) of the *Hopx* gene indicating the target positions of four gRNAs (**A**), and their efficiency to direct on-target cutting of a genomic 750-bp *Hopx* PCR product by Cas9 in vitro, as revealed by agarose gel electrophoresis (**B**). Arrow, uncut *Hopx* PCR product; bracket, fragments of cut *Hopx* PCR product. C, *Hopx* PCR product-only control with no gRNA added; M, DNA size markers as indicated on the right. Note the effectiveness of gRNA #10 and gRNA #13.

(**C-E**) In vivo specificity. Analysis of on- and off-target sites in PaprikaRFP-expressing cells isolated by FACS at E18.5 from mouse medNcx electroporated at E15.5 with either a plasmid encoding Cas9_T2A_PaprikaRFP and a gRNA targeting LacZ (control, ctrl; Kalebic et al., 2016), or with a mixture of two plasmids, each encoding Cas9_T2A_PaprikaRFP and one of the two gRNAs targeting Hopx (gHopx, either gRNA #10 or gRNA #13). Three embryos each were electroporated for control and gHopx, and the cells isolated from each set of embryos were pooled for analyses. (**C**) DNA sequencing analysis of amplicons containing either the *Hopx* site (*Hopx-1*) and 10 off-target sites (*OT1-10*) of gRNA #10 (~24,000 reads), or the *Hopx* site (*Hopx-2*) and 14 off-target sites (*OT11-24*) of gRNA #13 (~32,000 reads). Data are expressed as percentage of insertions and deletions at the *Hopx* sites and the respective predicted off-target sites as compared to the mouse genome reference sequence over the number

of aligned reads. Note that the frequency of mismatches at the predicted off-target sites upon gHopx electroporation was very low (<0.04%) and in the same range as the occurrence of mismatches at the two *Hopx* target sites upon control electroporation (<0.05% of ~50,000 reads). (**D**) Agarose gel electrophoresis of an amplicon containing both *Hopx* sites of gRNA#10 and gRNA #13. Arrow and arrowhead, *Hopx* PCR product without and with the deletion of the DNA sequence between the two *Hopx* target sites, respectively. Note the loss of the DNA between the two target sites in about 40% of cases (**E**) Quantification of the *Hopx* PCR product bands shown in **D**, expressed as a length-corrected intensity ratio of the lower band (with the ≈100 bp deletion) to the upper band (without the ≈100 bp deletion).

(**F**-**I**) Mouse E15.5 medNcx was *in utero* electroporated with either a plasmid encoding Cas9_T2A_PaprikaRFP and a gRNA targeting LacZ (control, Ctrl), or with a mixture of two plasmids, each encoding Cas9_T2A_PaprikaRFP and one of the two gRNAs targeting Hopx (gHopx, either gRNA #10 or gRNA #13), all under constitutive promoters, followed by analysis at E18.5. (**F**) Quantification of Hopx immunoreactivity in RFP+ cells in the VZ. (**G**,**H**) RFP (magenta) and PH3 (white) double immunofluorescence, combined with DAPI staining (blue), upon control (**G**) and gHopx (**H**) electroporation. White boxes in the left panels indicate the areas shown at higher magnification in the respective right panels. Arrows indicate basal RFP+ cells in mitosis, as revealed by PH3 immunofluorescence. Dashed lines indicate the boundary between ventricle and VZ. Images in left panels are 5-µm merged stacks (15 partly overlapping single 0.6-µm optical sections), images in right panels are single 0.6-µm optical sections; scale bars, 50 µm (left panels) and 10 µm (right panels). (**I**) Quantification of the percentage of RFP+ cells in the SVZ that are PH3+ upon control (grey column) and gHopx (black column) electroporation.

(**E**,**F**,**I**) Error bars indicate SD; *, *P* <0.05; Student's *t*-test in **F** (n = 3 embryos, *P* = 0.0.011, φ = 4, t = 4.50), Mann-Whitney's U test in **I** (n = 3 embryos, *P* = 0.0495). Open circles in the bar graphs represent individual data points.

Vaid et al., Fig. S8

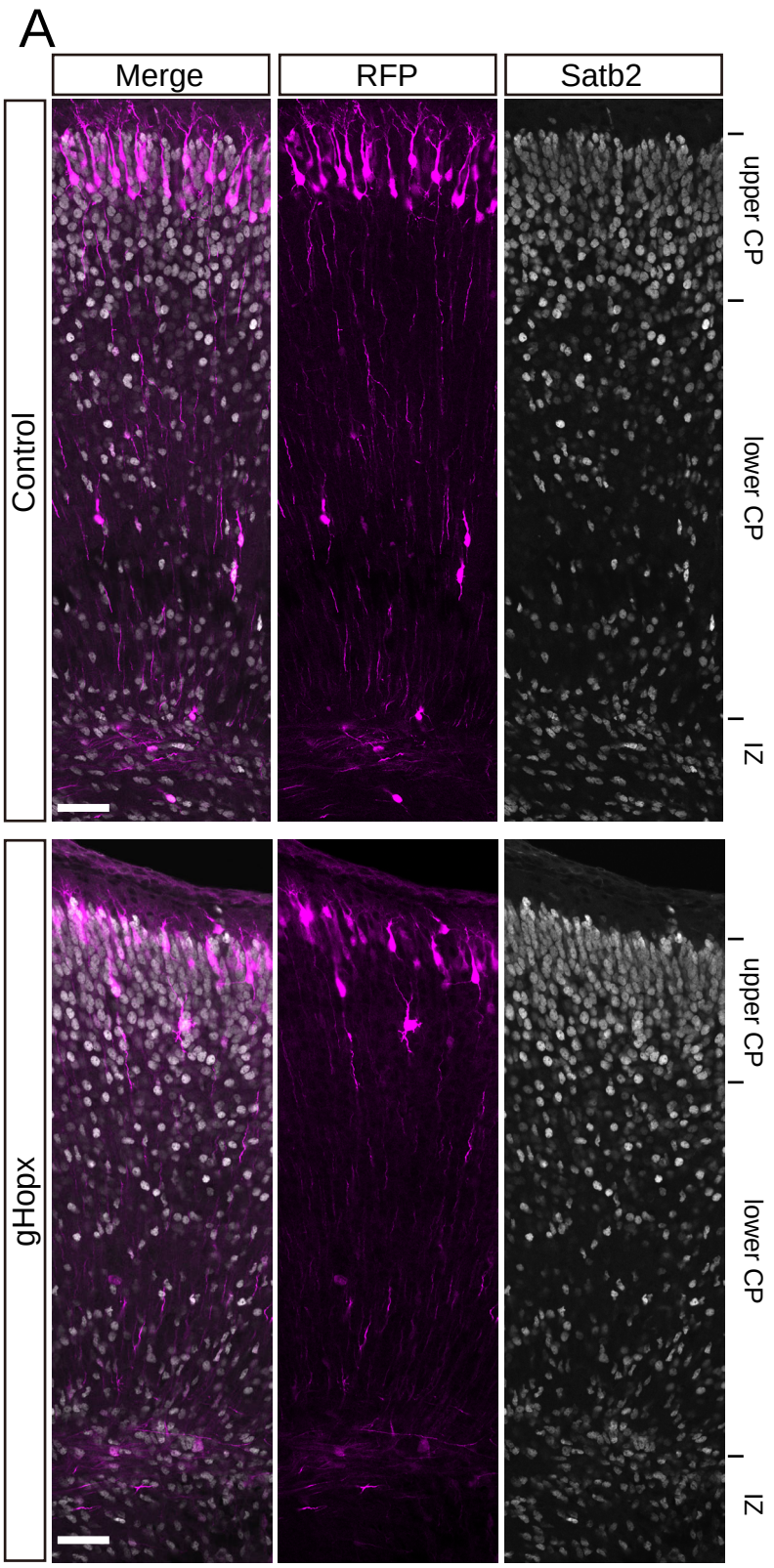

Figure S8. Effect of CRISPR/Cas9-mediated disruption of Hopx expression on neurogenesis in the early postnatal mouse neocortex.

We quantified the proportion of Satb2+ neurons among the progeny of the targeted cells (PaprikaRFP+) at P1. This analysis showed that disruption of Hopx expression in the embryonic mouse medNcx resulted in a significant, ~40% decrease in the proportion of the Satb2+ neurons that were still migrating to the CP upper layers, among the progeny of the targeted cells.

For this analysis, mouse E15.5 medNcx was *in utero* electroporated with either a plasmid encoding Cas9_T2A_PaprikaRFP and a gRNA targeting LacZ (control, Ctrl), or with a mixture of two plasmids, each encoding Cas9_T2A_PaprikaRFP and one of the two gRNAs targeting Hopx (gHopx, either gRNA #10 or gRNA #13), all under constitutive promoters, followed by analysis at P1.

(**A**) RFP (magenta) and Satb2 (white) double immunofluorescence, upon control (top) and gHopx (bottom) electroporation. Images are single 0.6-µm optical sections; scale bars, 50 µm.

(**B**) Quantification of the percentage of RFP+ cells in the wall of the medNcx (50 µm-wide microscopic field) that express Satb2, a marker of late-born neurons (Britanova et al., 2008; Molyneaux et al., 2015), and located in the lower CP, IZ and SVZ, i.e. newborn Satb2+ neurons that were still migrating to the CP upper layers at P1, upon control (grey column) and gHopx (black column) electroporation. Error bars indicate SD; *, P <0.05. Student's t-test (n = 5 (control) and 4 (gHopx) embryos, P = 0.0.04994, φ = 7, t = 2.37). Open circles represent individual data points.

Vaid et al., Fig. S9

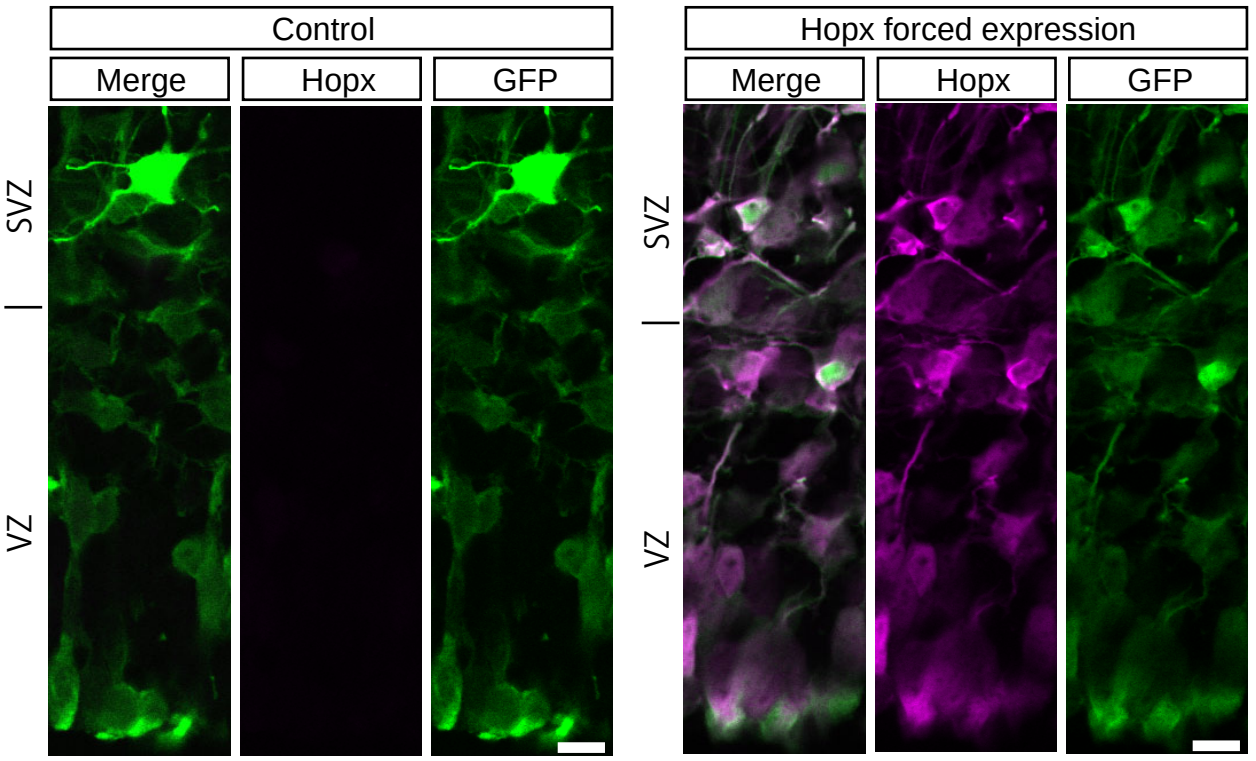

Figure S9. Presence of Hopx protein in the progeny of the electroporated cells upon forced Hopx expression in the embryonic mouse latNcx.

Mouse E15.5 latNcx was *in utero* co-electroporated with a plasmid encoding GFP together with either an empty vector (control) or a Hopx expression plasmid (Hopx forced expression), all under constitutive promoters, followed by analysis at E18.5. GFP (green) and Hopx (magenta) double immunofluorescence upon control (left) and Hopx forced expression (right). Images are 5-µm merged stacks (15 partly overlapping single 0.6-µm optical sections); scale bars, 10 µm.

Vaid et al., Fig. S10

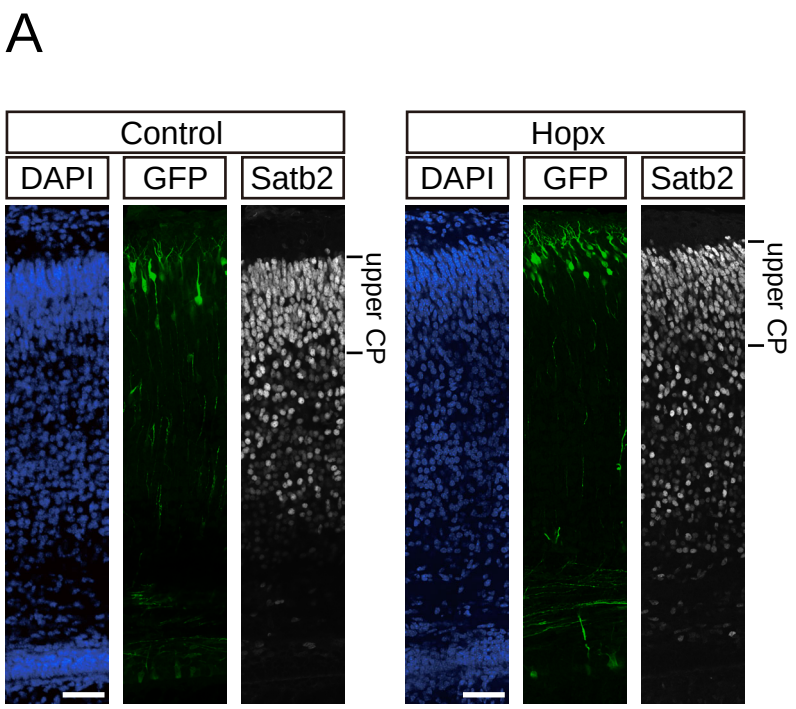

Figure S10. Effect of forced Hopx expression on neurogenesis in the early postnatal mouse neocortex.

We quantified the proportion of Satb2+ neurons among the progeny of the targeted cells (GFP+) at P1. This analysis showed that forced Hopx expression in the embryonic mouse latNcx initiated at E15.5 resulted in a significant, ~40% increase in the proportion of Satb2+ neurons that had arrived in the upper cortical layers, among the progeny of the targeted cells in the upper CP at P1.

For this analysis, mouse E15.5 latNcx was *in utero* co-electroporated with a plasmid encoding GFP together with either an empty vector (control, Ctrl) or a Hopx expression plasmid (Hopx), all under constitutive promoters, followed by analysis at P1.

(**A**) GFP (green) and Satb2 (white) double immunofluorescence, combined with DAPI staining (blue), upon control (left) and Hopx (right) electroporation. Images are single 0.6-µm optical sections; scale bars, 50 µm. Images are single 0.6-µm optical sections; scale bars, 50 µm.

(**B**) Quantification of the percentage of GFP+ cells in the wall of the latNcx (50 µm-wide microscopic field) that are Satb2+ and located in the upper CP, i.e. Satb2+ neurons that had arrived in the upper cortical layers by P1, upon control electroporation (grey column) and forced Hopx expression (black column). Error bars indicate SD; *, $P < 0.05$. Student's *t*-test (n = 4 embryos, $P = 0.036$, $\varphi = 6$, $t = -2.69$). Open circles represent individual data points.

Vaid et al., Fig. S11

A

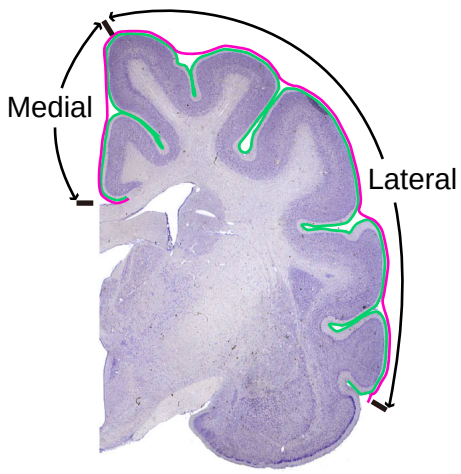

B

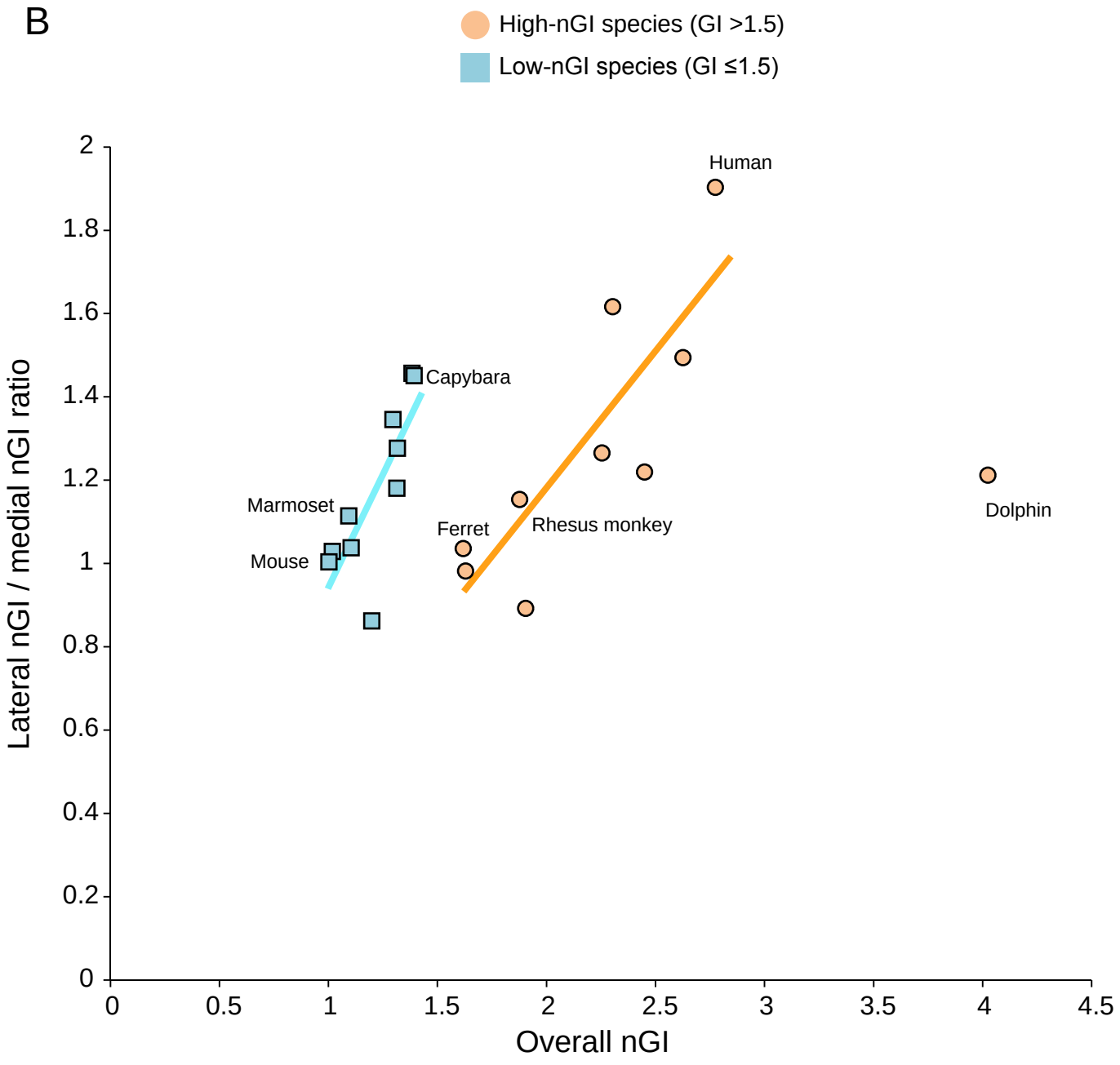

Figure S11. Increase in overall nGI among species is accompanied by an increase in the lateral nGI / medial nGI ratio.

(**A**) Illustration of the determination of the lateral nGI / medial nGI ratio. Coronal section of the neocortex of an adult *Felis catus* (obtained from http://neurosciencelibrary.org/); green line, inner contour; magenta line, outer contour. MedNcx and latNcx are indicated by double-headed arrows.

(**B**) Lateral nGI / medial nGI ratio as a function of overall nGI in the two principal groups of mammals (GI ≤1.5 vs. GI >1.5) (Lewitus et al., 2014). Blue squares, 10 selected low nGI (≤1.5) species (mouse (indicated), hedgehog, marmoset (indicated), manatee, bushbaby, owl monkey lemur, kangaroo, hyrax, capybara (indicated)); orange circles, 10 selected high nGI (>1.5) species (ferret (indicated), cat, rhesus monkey (indicated), fox, chimpanzee, boar, goat, seal, human (indicated), dolphin (indicated); blue line, regression analysis of the 10 low nGI species, $y = 1.083x - 0.137$, $R^2 = 0.63$, $P = 0.0059$; orange line, regression analysis the 9 high nGI species without the dolphin (studentized residual = 7.56), $y = 0.656x - 0.132$, $R^2 = 0.71$, $P = 0.0043$.

Table S1. Information of on- and off-target sites and probes

Amplicon name	On / off-target sequence	Locus	Chromosome	chromosome location		CFD Score*	primer-forward	primer-reverse
Hopx-1	CAGACGCGCACGGACCATGTCGG	Hopx	chr 5	77094960	77094979	1	AGGATCTCCACCTGGTCCTC	GGCCATCTGGTTCCCCTG
OT-1	CAGTCGTGCACAGACCATGTGGG	intergenic:Ccdc147-Sorcs3	chr19	48157623	48157717	0.48257576	CCATTATCAGGCGAGTGGAGG	CTCACTTTGGGGTAGGGCTG
OT-2	CAGAAACTCACGGACAATGTTGG	intergenic:Ccdc167-Mdga1	chr17	29775843	29775911	0.35714286	CCCTTCCCCGGGTAAGAAAC	GCCCTTCCCCTTTAACAGCT
OT-3	CAGACACCCAAGGACCATCTTGG	intergenic:C230014O12Rik-Pbx3	chr2	34170387	34170497	0.20689655	CAACAGACTGACCCAGGACA	TGAGCTGTGTGGTTTTGCAA
OT-4	CAGACTCTCAAGCACCATGTAGG	intron:9030622O22Rik	chr2	148009234	148009346	0.13157895	GGGGTGCTGGATCCTTTTGA	TCTATACAATGGACTGGGCAGA
OT-5	CAGTCTCACATGGACCATGTTGG	intergenic:Plch1-Gm16162	chr3	63806483	63806590	0.13053613	GAGAAGTAGGAGGCAGGGGA	CCCCTAACCTCACATGGCTC
OT-6	CAGAAGCTCACGGGCCATCTAGG	intergenic:Gm24504-Nedd4l	chr18	64804093	64804199	0.07471264	GGGTGTGTATTGGGTATGTGC	ACAGGAACCAGAGACCGAGA
OT-7	CAGAAGCACAGGGACCATCTAGG	intergenic:Adra2a-Gpam	chr19	54583375	54583463	0.06403941	TGTGAGTGTTCATCTCTGGATGG	TTTTGCTCCTCTCCAACCCC
OT-8	CAGAGGTGCACGGAACATCTGGG	intergenic:Gm26489-1700028P15Rik	chr2	171592476	171592498	0.04856322	CACCAGGCTTGTGGGAGATT	AGCCAGCAGTATGGATCGTG
OT-9	CAGACAGGCATGGACTATGTTGG	intergenic:Gm8349-Arhgef26	chr3	61664889	61664991	0.04455273	TGTGACAGTGCCATTTGAGAGA	CCTCTGGCACACCTACCAAC
OT-10	CAGAGGGGCAGCGACCATGTTGG	exon:Map1a	chr2	121301773	121301903	0.03737024	CAGCCAGTCTGCAGAGAGTG	TGGCTGAGGACACATGTTCC
Hopx-2	GACCCGCCTCGGCTGCGATGAGG	Hopx	chr 5	77094848	77094979	1	ATAGGCTTGGGGACTCACCT	GAGGACCAGGTGGAGATCCT
OT-11	TAACCACCTCAGCTGCGATGAGG	exon:1700026L06Rik	chr2	28693019	28693041	0.86666667	CGCCTCCATAGTGGTTCCTG	CCACCTGCTCACTATCCTGC
OT-12	AAACTGCCCCGGCTGCGATGGGG	exon:Reep6	chr10	80335486	80335508	0.45818182	CCAGATTCCCAGCAAGTCCC	AGAGTCCCACTGGGCAGTC
OT-13	GCCACGCGCCGGCTGCGATGGGG	intergenic:Prkcb-Cacng3	chr7	122649519	122649541	0.39262993	TCCCCTCGTCTATGCCTTCA	TGGGTGGGCATAGCAACAG
OT-14	GAACCACCTCAGCTGCGAAGAGG	intron:Wdfy3	chr5	101883241	101883263	0.24761905	CCCAGCACTAGAGTTCTGGC	ACTGTGGCACTTCTGGCTTT
OT-15	GCTCCGCCTCGGCCGCGATGAGG	intergenic:Fabp5-Gm9833	chr3	10088140	10088162	0.15433673	AAACTTCAAAAGCGTCCGGC	CCTCGGACTTGTCGGCATC
OT-16	GCTCCGCCTCGGCCGCGATGAGG	exon:Myef2	chr2	125123529	125123551	0.15433673	CCTCGGACTTGTCGGCATC	GCTCGGGGCCTTTTCAAATC
OT-17	GACCTGCCTGGGCTGCAGTGTGG	intron:Erg	chr16	95446484	95446612	0.09239057	TGTCAAAGTTGCCCAGACTGT	CCAGTTCCCAGCCTTGAGAC
OT-18	GACTCGTCTCTGCTGTGATGTGG	intergenic:Gm25431-Ighmbp2	chr19	3160762	3160678	0.07692308	CCCATCACAAGGCCCATCAA	TGTAAGGCTGTTTTGCGTGG
OT-19	GTTCGGCCTCGGCTGCGAGGCGG	exon:Smarce1	chr11	99230283	99230305	0.075	CTGTTCCGGACGGGGTTG	GTGGTGTTTCTGCTTGGCG
OT-20	GCCCCGCCGCTTCTGCGATGTGG	intron:Nudt15	chr14	73524725	73524747	0.07195186	CTGACTTAGCTACCCTTCCCC	GGGACTTTTCCTTTTGCCCC
OT-21	GTCCCGCCTCCCCTGCGATCCGG	exon:Decr1	chr4	15945294	15945316	0.0707192	CTGCCTTACCCTCTGAGGAC	TGAGTCCTGCTGCAGACATG
OT-22	GACCCACCTCGGGTGAGTTGGGG	exon:Aplp2	chr9	31161748	31161770	0.06818182	AGCAGGCAACACTAAGAACA	CCGACGCATAGCTCTGGAAA
OT-23	GACCAGGCTGGGCTGCGTTGAGG	intron:Dlg4	chr11	70029326	70029348	0.05228758	CGCCCTGCAGTTTAGCTAGA	AAAGGGTTAAAGCGAGGCGT
OT-24	GACTCACCTCGGCTTCGGTGGGG	intron:Slc6a6	chr6	91697120	91697142	0.04571429	GCCTCACCCGTTGCAGATAT	GAAGTCACTGGGCCTTCCTC
							*Cutting Frequency Determination (CFD) score	

Supplementary references

Britanova, O., de Juan Romero, C., Cheung, A., Kwan, K. Y., Schwark, M., Gyorgy, A., Vogel, T., Akopov, S., Mitkovski, M., Agoston, D. et al. (2008). Satb2 is a postmitotic determinant for upper-layer neuron specification in the neocortex. *Neuron* **57**, 378-392.

De Juan Romero, C., Bruder, C., Tomasello, U., Sanz-Anquela, J. M. and Borrell, V. (2015). Discrete domains of gene expression in germinal layers distinguish the development of gyrencephaly. *EMBO J.* **34**, 1859-1874.

Florio, M., Albert, M., Taverna, E., Namba, T., Brandl, H., Lewitus, E., Haffner, C., Sykes, A., Wong, F. K., Peters, J. et al. (2015). Human-specific gene ARHGAP11B promotes basal progenitor amplification and neocortex expansion. *Science* **347**, 1465-1470.

Lewitus, E., Kelava, I., Kalinka, A. T., Tomancak, P. and Huttner, W. B. (2014). An adaptive threshold in mammalian neocortical evolution. *PLoS Biol.* **12**, e1002000.

Molyneaux, B. J., Goff, L. A., Brettler, A. C., Chen, H. H., Brown, J. R., Hrvatin, S., Rinn, J. L. and Arlotta, P. (2015). DeCoN: genome-wide analysis of in vivo transcriptional dynamics during pyramidal neuron fate selection in neocortex. *Neuron* **85**, 275-288.

Pollen, A. A., Nowakowski, T. J., Chen, J., Retallack, H., Sandoval-Espinosa, C., Nicholas, C. R., Shuga, J., Liu, S. J., Oldham, M. C., Diaz, A. et al. (2015). Molecular Identity of Human Outer Radial Glia during Cortical Development. *Cell* **163**, 55-67.